symmetry

MDPI

Article

A Chaotic Jerk Oscillator with Complete Control via Fractional Exponentiation and Its Experimental Analog Circuit Realization

Menghui Shen [1], Chunbiao Li [1,2,*], Xiaoliang Cen [1], Manyu Zhao [3], Yuanxiao Xu [4] and Ludovico Minati [3,5]

[1] School of Electronic and Information Engineering, Nanjing University of Information Science and Technology, Nanjing 210044, China; 202312490204@nuist.edu.cn (M.S.); xiaoliangcen@nuist.edu.cn (X.C.)
[2] School of Artificial Intelligence, Nanjing University of Information Science and Technology, Nanjing 210044, China
[3] School of Life Science and Technology, University of Electronic Science and Technology of China, Chengdu 611731, China; mzhao@mailbox.org (M.Z.); lminati@uestc.edu.cn (L.M.)
[4] Digital City Intelligence Research Institute, China Information Consulting & Designing Institute Co. Ltd., Nanjing 210019, China; xuyuanxiao@cicdi.cn
[5] Center for Mind/Brain Sciences (CIMeC), University of Trento, 38123 Trento, Italy
* Correspondence: goontry@126.com or chunbiaolee@nuist.edu.cn; Tel.: +86-139-1299-3098

Abstract: By introducing fractional exponentiation into a three-dimensional chaotic system, a jerk system with only six terms is designed. It has the property of total amplitude control, where a single non-bifurcation parameter can directly rescale all system variables without affecting the dynamics. It also features two-dimensional offset boosting, where a single parameter can realize direct offset boosting while another provides interlocked cross-dimensional offset boosting. Furthermore, this jerk system has a parameter-dominated symmetric attractor, which means that symmetric attractors appear successively as the parameter changes from positive to negative. Circuit experiments confirm the feasibility of analog fractional exponentiation using the 444 circuit and the complete control, including amplitude control and offset boosting, of the resulting system. The proposed circuit may facilitate applications of chaotic signal generators where signal versatility is important and exemplifies the generative potential of analog fractional exponentiation.

Keywords: amplitude boosting; complete control; 444 circuit; fractional exponentiation; jerk system; offset boosting

Academic Editor: Vasilis K. Oikonomou

Received: 30 December 2024
Revised: 21 January 2025
Accepted: 22 January 2025
Published: 24 January 2025

Citation: Shen, M.; Li, C.; Cen, X.; Zhao, M.; Xu, Y.; Minati, L. A Chaotic Jerk Oscillator with Complete Control via Fractional Exponentiation and Its Experimental Analog Circuit Realization. *Symmetry* **2025**, *17*, 174. https://doi.org/10.3390/sym17020174

1. Introduction

Chaos is a peculiar form of motion that is ubiquitous in natural and artificial nonlinear dynamic systems across scales of time and space, representing an interface between determinism and randomness, regularity, and complexity. To date, a plethora of chaotic systems have been discovered, such as the Lorenz system [1,2], the Chua system [3,4], and the Rössler system [5,6]. Based on the computational enumeration method, Sprott proposed a class of simple third-order autonomous chaotic systems known as jerk systems. Such systems find widespread applications in control and signal processing systems and are currently the subject of active research. Their equation takes the general form $\dddot{x} = J(x, \dot{x}, \ddot{x})$, where represents $\dot{x}$ velocity, $\ddot{x}$ is acceleration, and $\dddot{x}$ is jerk. In 1997, Sprott proposed some standard forms and the simplest quadratic form of jerk systems [7]. Subsequently, notable results have been obtained by modifying chaotic systems based on jerk equations and uncovering different types of dynamics, such as coexisting attractors [8], multi-scroll attractors [9], and hyperchaos [10].

In addition, much research has been conducted on shaping chaotic dynamics through amplitude control and offset boosting. A chaotic system that possesses both of these controls is said to offer complete control [11]. Several studies have shown that in suitable chaotic systems, the amplitude and direction of the chaotic orbits and corresponding signals can be freely controlled by independent non-bifurcation parameters. In particular, amplitude control provides a convenient means of rescaling signals, allowing the generation of chaotic signals with the desired amplitude adjusted by a single knob [12,13]. On the other hand, offset boosting allows chaotic signals to arbitrarily switch between bipolar and unipolar states by introducing an independent constant that can move the variables to any position in phase space [14,15]. When chaotic systems are used in large-scale networks, such as networks that replicate neural connectomes, or in practical engineering applications, such as mixing and steering control, the simple control of the size and location of the attractor, independent of its geometry, provides maximum flexibility [16]. In this paper, we construct a chaotic system that provides full amplitude control and two-dimensional offset boosting, where non-bifurcation parameters realize full control over the size and location of the attractor.

As the properties of chaotic dynamics have been progressively revealed, the diligent performance of circuit experiments has become an indispensable step, not only to confirm the viability of numerical simulations but also to discover entirely new phenomena. In addition, experiments are of paramount importance to reveal the effects of component non-idealities and tolerances, which are ubiquitous in physical devices but difficult to represent in numerical simulations. Circuit experiments are also a prerequisite for demonstrating the applicability of chaotic systems in engineering practice. For example, the Chua circuit [17], which is well-known as a basis for implementing chaos via analog circuits, is structurally simple and requires only a handful of components. If the state equations of a system are known, a modular design approach can be used to design a corresponding analog circuit, using basic elements such as adders, subtractors, multipliers, integrators, and inverters to implement prescribed algebraic relations [18,19]. This method is versatile, but it often results in circuits that are significantly larger than those discovered by serendipity or from first principles, which may be as simple as requiring only a single transistor. In recent years, many researchers have pursued simplifications of chaotic circuits and systems [20,21].

For example, a jerk circuit based on the absolute value function was implemented by Li et al. [22] using diodes and operational amplifiers, while Wu et al. utilized the coupling of capacitors and resistors along with the inherent characteristics of multipliers to realize compact quadratic computation and generate chaos [23]. In some circumstances, chaos can be produced in fractional order systems [24,25] or even resort to the feedback of fractional exponentiation. In this paper, the circuit implementation of a three-dimensional jerk system has been optimized by exploiting the characteristics of a positive-phase integrator with only a minimal number of operational amplifiers and linear components while incorporating a novel circuit that realizes fractional exponentiation. This circuit structure is highly advantageous for advancing future research on memristive chaotic systems as well as in-depth studies of neural dynamics [26]. The novelty concerns the following aspects:

(1) The overall amplitude control parameter is discovered in the designed chaotic oscillator, allowing one to directly influence the amplitude of all system variables;
(2) Two offset parameters are identified, one realizing offset amplification along one dimension and the other providing cross-dimensional offset amplification;
(3) Fractional exponentiation is achieved in the analog domain using logarithmic and exponential operation modules as building blocks, exploiting the nonlinear response of bipolar transistors, according to a newly introduced circuit known as the 444 circuit;
(4) A detailed experimental characterization is undertaken.

The remainder of this paper is organized as follows. In Section 2, the model and dissipative analysis are provided. In Section 3, the dynamic behavior is analyzed. In Section 4, the possibilities of amplitude control and offset boosting are introduced. In Section 5, the system is implemented using a simplified analog electronic circuit, yielding experimental results consistent with theoretical analysis and numerical simulations. Finally, Section 6 provides a concluding summary.

2. System Definition

Based on the notion that nonlinear feedback is the fundamental prerequisite for chaos generation in dynamic systems, a modification of the jerk system MO_4 [27] was made by introducing fractional exponentiation, namely,

$$\begin{cases} \dot{x} = y, \\ \dot{y} = az, \\ \dot{z} = -z - cy + |y|_b - x. \end{cases} \tag{1}$$

The original system of MO_4 has only a single nonlinear quadratic term x^2, and it includes another linear term of x, which provides the possibility to replace the nonlinear term with a fractional exponentiation of $|x|^b$. For the controllability of two-dimensional offset boosting, we further revise the feedback $|x|^b$ with $|y|^b$, which happens to be satisfied by another linear feedback of y. In this system, a, b, and c are the system parameters, assumed to be constant, while x, y, and z are the state variables. The system comprises five linear terms and one nonlinear term. When its parameters are set to $a = 1$, $b = 2.4$, and $c = 0.6$, given the initial condition (0, 0.1, 0), the Lyapunov exponents (LEs) are found to be (0.0527, 0, −1.0527), and the Kaplan–Yorke dimension (D_{KY}) is consequently 2.05. The corresponding chaotic attractor obtained by integrating the system using a variable-step fourth-order Runge–Kutta method is shown in Figure 1.

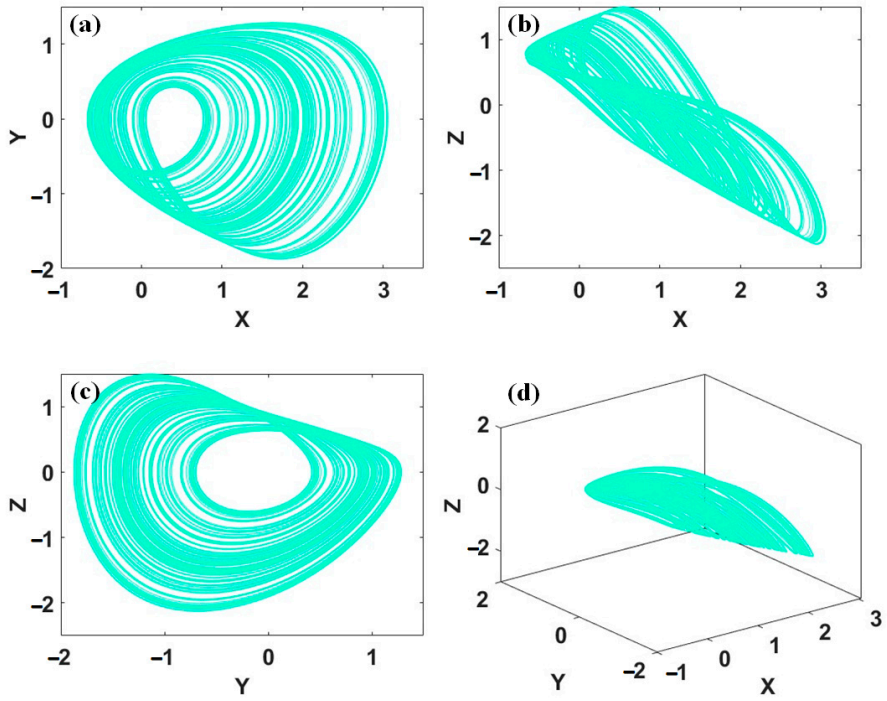

Figure 1. Phase portraits obtained by integrating Equation (1), given $a = 1$, $b = 2.4$, and $c = 0.6$, and the initial condition (0, 0.1, 0): (**a**) x–y projection; (**b**) x–z projection; (**c**) y–z projection; and (**d**) x–y–z space.

As Equation (1) represents a jerk system, it can be rewritten more compactly as a third-order differential equation, namely,

$$\dddot{x} = -\ddot{x} - ac\dot{x} + a|\dot{x}|^b - ax. \tag{2}$$

3. Dynamical Analysis

3.1. Equilibrium Points and Stability

Let $\dot{x} = 0$, $\dot{y} = 0$, $\dot{z} = 0$, yielding the following:

$$\begin{cases} y = 0, \\ az = 0, \\ -z - cy + |y|^b - x = 0. \end{cases} \tag{3}$$

When the parameter settings are taken as $a = 1$, $b = 2.4$, and $c = 0.6$, the system in Equation (1) has only one equilibrium point. In order to obtain the eigenvalues of the equilibrium point and determine its stability, the Jacobian matrix at the equilibrium point S_0 (0, 0, 0) can be obtained, giving the following:

$$J = \begin{bmatrix} 0 & 1 & 0 \\ 0 & 0 & a \\ -1 & -c + b|y|^{b-1}\mathrm{sgn}(y) & -1 \end{bmatrix} \tag{4}$$

Thereafter, the characteristic equation can be written as

$$\lambda^3 + \lambda^2 + c\lambda + 1 = 0 \tag{5}$$

from which the eigenvalues are found to be $\lambda_1 = -1.1968$, $\lambda_2 = 0.0984 + 0.9088i$, and $\lambda_3 = 0.0984 - 0.9088i$. Therefore, S_0 is a saddle-focus point of index 2.

3.2. Bifurcation Analysis

To analyze the sensitivity to parameter changes, let $a = 1$ and $c = 0.6$, with an initial condition of (0, 0.1, 0). When the parameter b varies within the interval [1.5, 3], its Lyapunov exponents and bifurcation diagram evolve as depicted in Figure 2. It can be observed that when the parameter b increases, the system undergoes multiple transitions between periodic and chaotic states. In particular, periodic orbits are found within the intervals [1.5, 1.809], [1.58, 2.162], and [2.162, 2.248] and are followed by transitions to chaotic states through period-doubling bifurcations. Its typical phase trajectory is shown in Figure 3, and the LEs and D_{KY} values are presented in Table 1. However, as the parameter b approaches 3, the system tends to diverge, leading to the inability to generate chaotic behavior. The sign of the largest Lyapunov exponent shows good agreement with the chaotic regions in the bifurcation diagram.

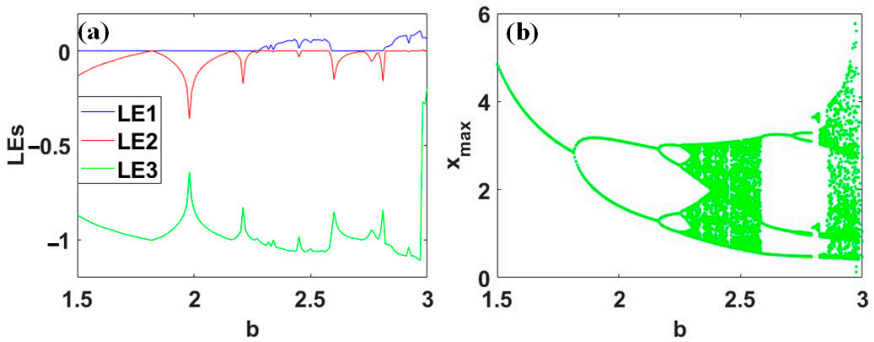

Figure 2. Dynamics observed in Equation (1), with $a = 1$, $c = 0.6$, and an initial condition of (0, 0.1, 0) while the parameter b varies over [1.5, 3]: (**a**) Lyapunov exponents and (**b**) bifurcation diagram.

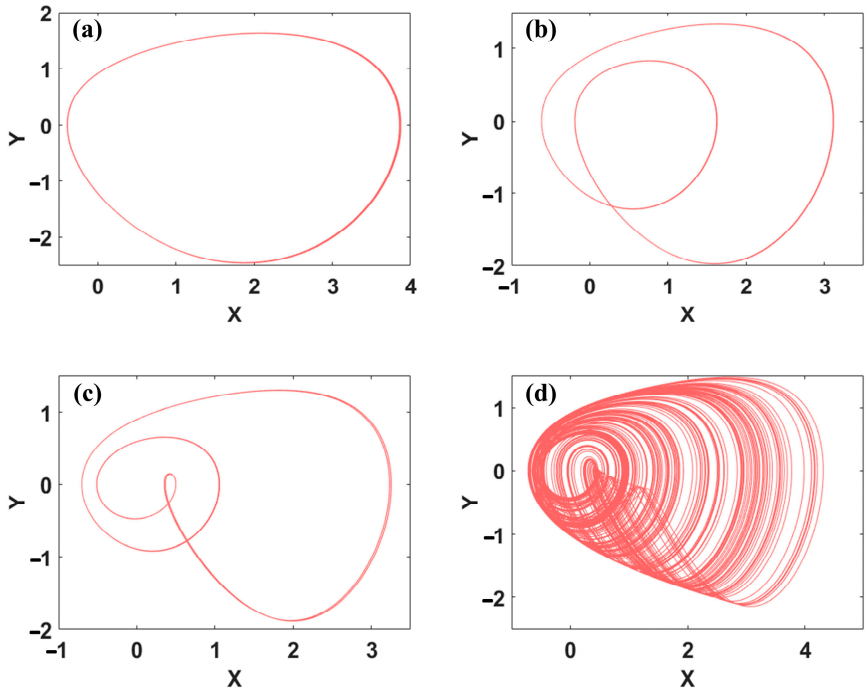

Figure 3. Representative phase portraits obtained with $a = 1$, $c = 0.6$, and the initial condition (0, 0.1, 0) for (**a**) $b = 1.6$; (**b**) $b = 2$; (**c**) $b = 2.7$; and (**d**) $b = 2.9$.

Table 1. Summary of the dynamic parameters obtained with $a = 1$, $c = 0.6$, and the initial condition (0, 0.1, 0).

b	Attractor	Lyapunov Exponents	D_{KY}
1.6	period 1	(0, −0.0744, −0.9256)	1
2.0	period 2	(0, −0.1663, −0.8337)	1
2.7	period 3	(0, −0.0029, −0.9961)	1
2.9	chaos	(0.0746, 0, −1.0746)	2.07

When the parameter b is fixed at 2.4 and the initial values are (0, 0.1, 0), the Lyapunov exponent spectrum and bifurcation diagram for parameter a varying within the interval [0.2, 1.8] appear as depicted in Figure 4. It is observed that as this parameter increases, the system again undergoes multiple transitions between chaotic and periodic states, yielding the attractor exemplified in Figure 5.

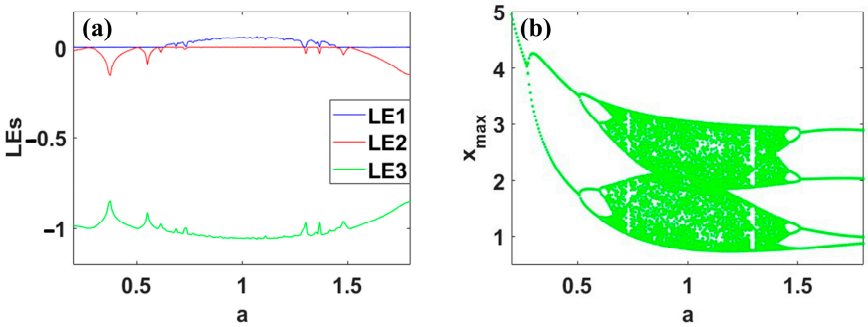

Figure 4. Dynamics with $b = 2.4$, $c = 0.6$, and the initial condition (0, 0.1, 0) while a varies over [0.2, 1.8]: (**a**) Lyapunov exponents and (**b**) bifurcation diagram.

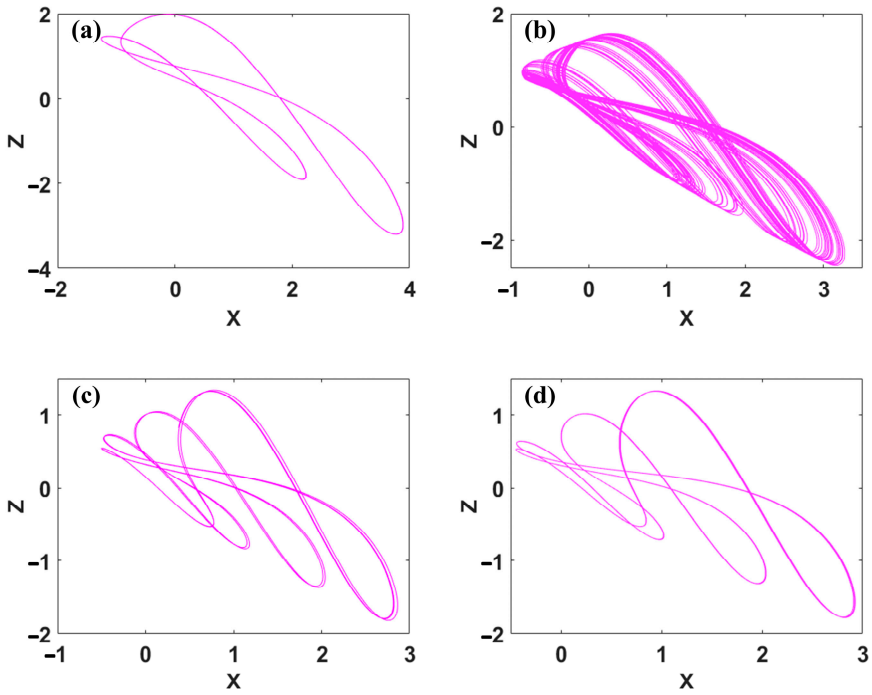

Figure 5. Representative phase portraits obtained with $b = 2.4$, $c = 0.6$, and the initial condition (0, 0.1, 0): (**a**) $a = 0.6$ (period 2); (**b**) $a = 0.7$ (chaos); (**c**) a = 1.45 (period 7); and (**d**) a = 1.7 (period 4).

4. Complete Control

4.1. Amplitude Control

When $a = 1$, following the substitutions $x \to n^{\frac{1}{b-1}}x$, $y \to n^{\frac{1}{b-1}}y$, $z \to n^{\frac{1}{b-1}}z$. $(n > 0)$, Equation (1) can be rewritten as

$$\begin{cases} \dot{x} = y, \\ \dot{y} = az, \\ \dot{z} = -z - cy + n|y|_b - x. \end{cases} \tag{6}$$

It can be observed that the coefficient in front of $|y|^b$ enables global amplitude control over x, y, and z. In other words, changes in the parameter n scale the state variables x, y, and z proportionally. Since $|y|^b$ is the only nonlinear term in the system, the value of n cannot be zero. At the same time, parameter b serves as the bifurcation parameter for the entire system. By adjusting its value, one can effectively control the amplitude effect of the non-bifurcation parameter n. As shown in Figure 6a, when the parameter n takes values within the range [0.1, 10] while other parameters are fixed, the average magnitudes of the state variables x, y, and z decrease as parameter n increases. Figure 6b illustrates the Lyapunov exponent spectrum of the system when n varies over the interval [0.1, 10]. It is confirmed that varying this parameter does not influence the Lyapunov exponents, indicating the absence of geometric changes in the chaotic trajectories. Some examples of the attractors obtained for different settings of the parameter n are depicted in Figure 7.

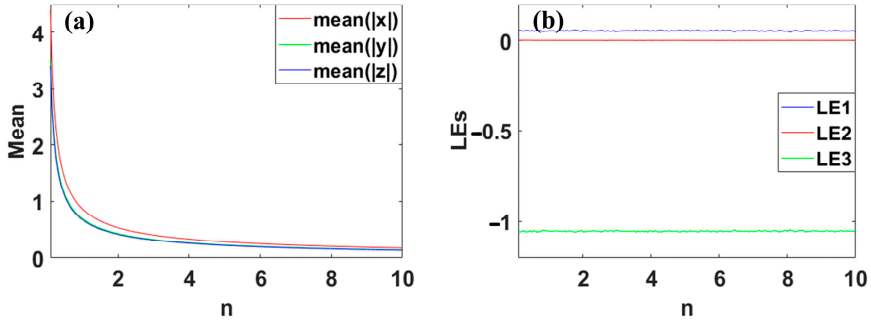

Figure 6. Amplitude evolution observed with $a = 1$, $b = 2.4$, $c = 0.6$, and the initial condition (0, 0.1, 0) as n varies over [0.1, 10]: (**a**) rescaled average magnitude and (**b**) Lyapunov exponents.

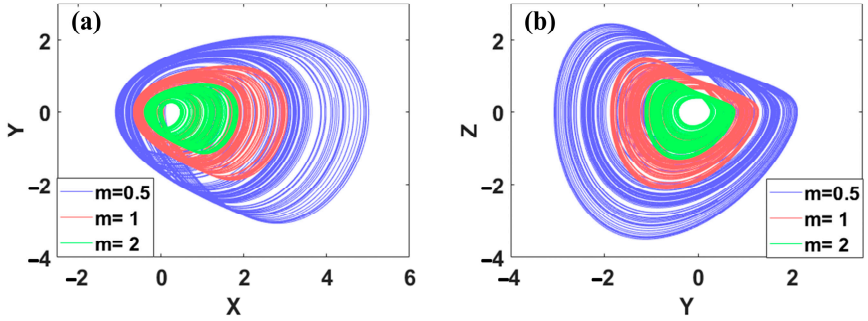

Figure 7. Demonstration of amplitude control with $a = 1$, $b = 2.4$, $c = 0.6$, and the initial condition (0, 0.1, 0): (**a**) x–y projection and (**b**) y–z projection.

When $x \to -n^{\frac{1}{b-1}}x$, $y \to -n^{\frac{1}{b-1}}y$, $z \to -n^{\frac{1}{b-1}}z.(n > 0)$, Equation (6) can be rewritten as

$$\begin{cases} \dot{x} = y, \\ \dot{y} = az, \\ \dot{z} = -z - cy - n|y|_b - x. \end{cases} \tag{7}$$

When the feedback of fractional exponentiation becomes negative, its phase trajectories are as shown in Figure 8, which is equivalent to inverting all the variables, thus achieving symmetry of the attractor around the origin.

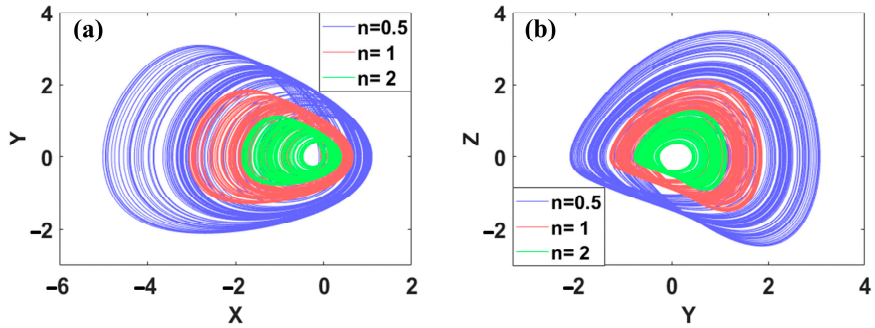

Figure 8. Attractor projections under different values of parameter n with $a = 1$, $b = 2.4$, $c = 0.6$, and the initial condition (0, −0.1, 0): (**a**) x–y projection and (**b**) y–z projection.

4.2. Two-Dimensional Offset Boosting

Let us consider two parameters d_1 and d_2, which provide offset boosting over the system variables x and z. The parameter d_1 controls the offset of the variables x and z in opposite directions, while parameter d_2 directly controls the variable x. These parameters are added, respectively, to the second and third dimensions of Equation (1).

$$\begin{cases} \dot{x} = y, \\ \dot{y} = az + d_1, \\ \dot{z} = -z - cy + |y|^b - x + d_2. \end{cases} \tag{8}$$

When replaced with $x \to x + \frac{d_1}{a} + d_2$, $y \to y$, $z \to z - \frac{d_1}{a}$, Equation (8) reverts to Equation (1), indicating that the introduced constants do not alter the system structure but provide opportunities for offset boosting the variables x and z.

First, when $d_1 = 0$, $d_2 \neq 0$, offset boosting over the variable x is achieved. The result of the replacement is $x \to x - d_2$, $y \to y$, $z \to z$, indicating that a single parameter d_2 added to the third dimension of Equation (1) offers independent offset boosting of variable x without any change in the dynamics, as illustrated in Figure 9.

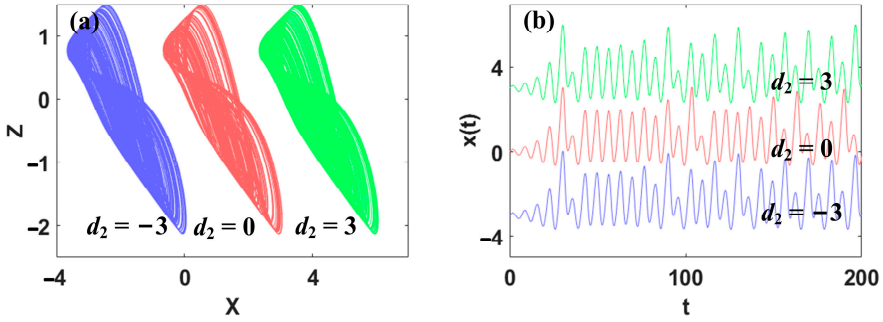

Figure 9. Offset boosting along the dimension of variable x in Equation (8) when $d_1 = 0$ given the initial condition (d_2, 0.1, 0): (**a**) x–z projection and (**b**) time series of $x(t)$.

Second, when $d_1 \neq 0$, $d_2 = 0$, offset boosting along the dimensions of variables x and z is achieved. The result of the replacement is $x \to x - \frac{d_1}{a}$, $y \to y$, $z \to z + \frac{d_1}{a}$, indicating that a single parameter d_1 introduced in the second dimension of Equation (1) performs cross-dimensional interlocked offset boosting over variables x and z in opposite directions, while the variable y remains unchanged, as illustrated in Figure 10.

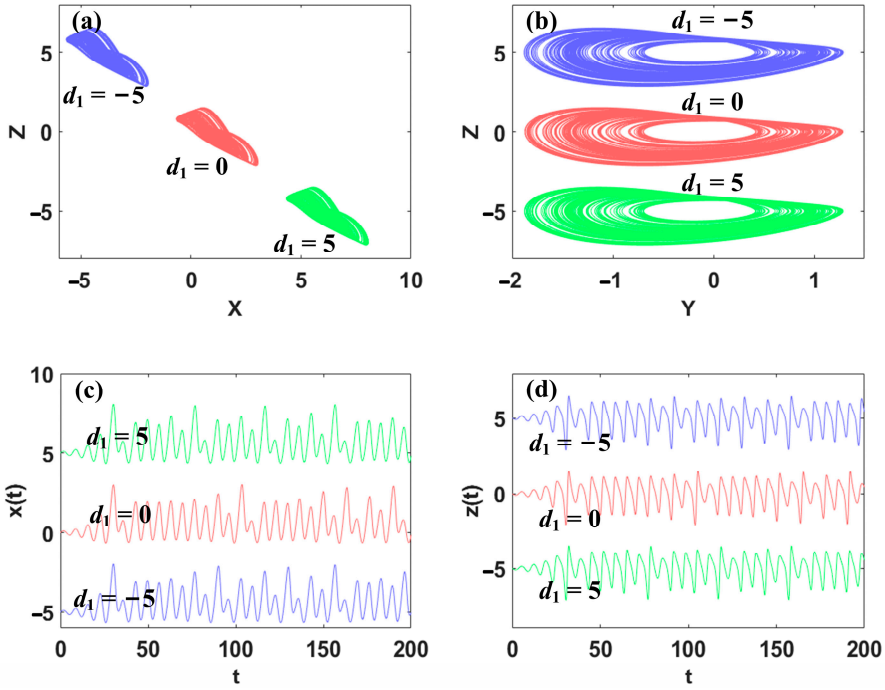

Figure 10. Interlocked offset boosting of Equation (8) with $d_2 = 0$ given the initial condition (d_1, 0.1, $-d_1$): (**a**) x–z projection; (**b**) y–z projection; (**c**) time series of $x(t)$; and (**d**) time series of $z(t)$.

Third, when $d_1 = -ad_2 \neq 0$, offset boosting along the dimension of z is achieved. The result of the replacement is $x \to x$, $y \to y$, $z \to z - d_2$, indicating that the addition of constrained variables in the second and third dimensions allows for independent offset boosting over the variable z, as illustrated in Figure 11.

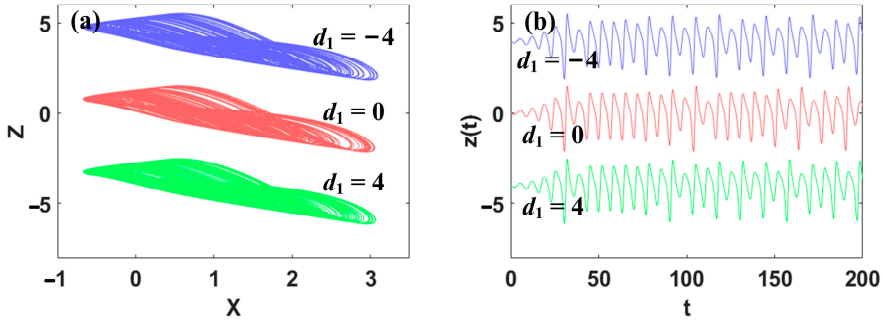

Figure 11. Offset boosting along the dimension of variable z of Equation (8) with $d_1 = -ad_2$ under the initial condition $(0, 0.1, -d_1)$: (**a**) x–z projection and (**b**) time series of $z(t)$.

Finally, when $d_1 \neq 0$, $d_2 \neq 0$, the offset boosting in Equation (1) is derived from $x \to x - \frac{d_1}{a} - d_2$, $y \to y$, $z \to z + \frac{d_1}{a}$, resulting in differential offset boosting over the variables x and z, as illustrated in Figure 12.

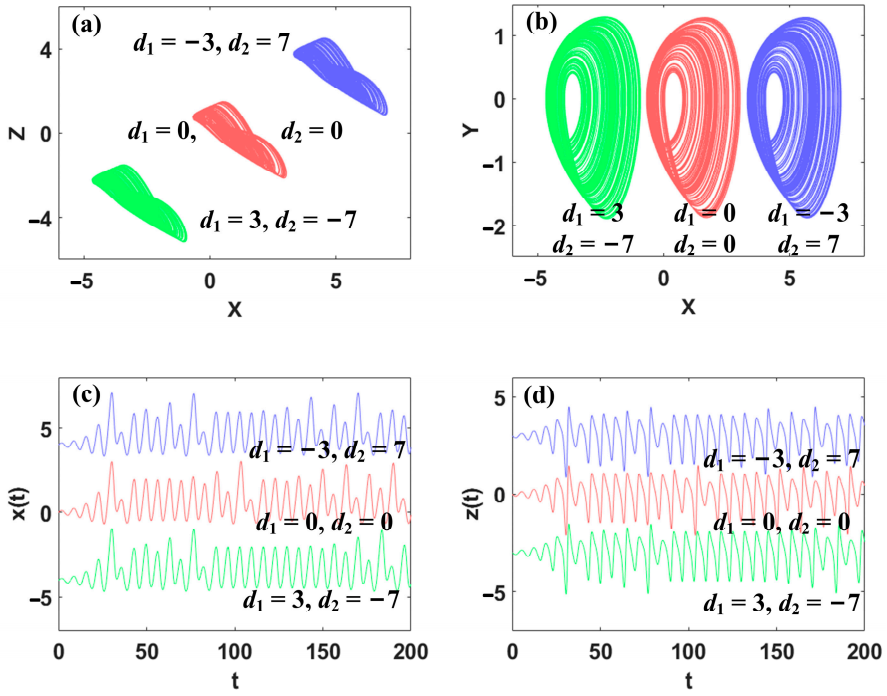

Figure 12. Differential offset boosting of Equation (8) under the initial condition $(d_1 + d_2, 0.1, -d_1)$: (**a**) x–z projection; (**b**) x–y projection; (**c**) time series of $x(t)$; and (**d**) time series of $z(t)$.

To better illustrate the aforementioned properties, when $d_1 = 0$, $d_2 \neq 0$, with changes in parameter d_2, the mean values of each system variable are depicted in Figure 13a. It can be observed that the average value of variable x increases proportionally, while the averages of y and z remain constant, indicating that variations in parameter d_1 do not induce offset boosting over dimensions x and z. Similarly, when $d_1 \neq 0$, $d_2 = 0$, the mean values of the variables x and z exhibit proportional changes in opposite directions, with variations in parameter d_1, while the mean value of y remains stable, as illustrated in Figure 13b. When $d_1 \neq -ad_2 \neq 0$ and $a = 1$, it is observed that only the average value of variable z changes, confirming the achievement of independent offset boosting over variable z. When

$d_1 \neq 0$, $d_2 \neq 0$, the scenario of $d_1 = d_2$ is selected, resulting in mean values depicted in Figure 13d. The offset boosting over variables x and z can be adjusted arbitrarily. In conclusion, changes in the proposed parameters do not affect the dynamic behavior of the system, and the resulting flexibility appears remarkable.

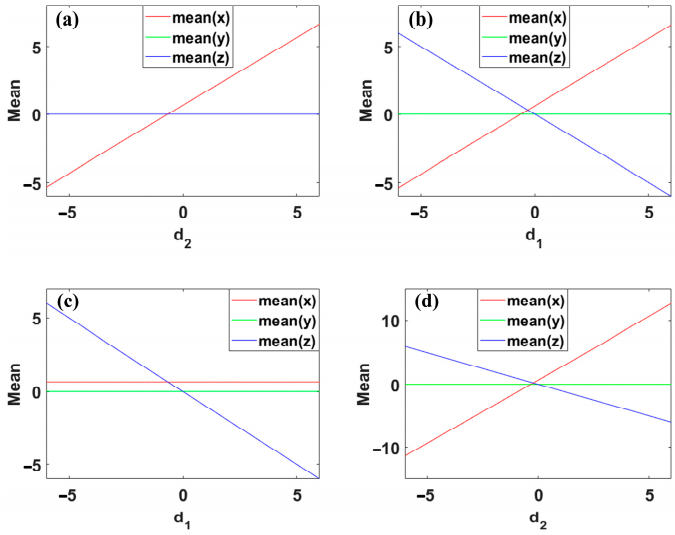

Figure 13. Differential offset boosting in Equation (8): (**a**) initial condition (d_2, 0.1, 0), $d_1 = 0$, $d_2 \in [-6, 6]$, (**b**) initial condition (d_1, 0.1, $-d_1$), $d_2 = 0$, $d_1 \in [-6, 6]$, (**c**) initial condition (0, 0.1, $-d_1$), $d_1 = -d_2 \in [-6, 6]$, and (**d**) initial condition ($2d_2$, 0.1, $-d_2$), $d_1 = d_2 \in [-6, 6]$.

5. Analog Electronic Circuit Experiments

5.1. Circuit Design and Experimental Setup

To demonstrate the practical feasibility of the system and its control, an analog computer was designed following the integrated design approach described in Ref. [28]. In other words, the corresponding algebraic relations were implemented by means of circuits based on operational amplifiers, namely integrations. The fractional exponentiation operation at the heart of the nonlinear feedback in the proposed system, which is notoriously difficult to realize in the analog domain, was provided by the 444 circuit, a newly introduced topology described in Ref. [29].

Based on Kirchoff's current and voltage laws, the circuit equations can be straightforwardly written as

$$\begin{cases} \dot{x} = \frac{y}{R_1 C_1}, \\ \dot{y} = \frac{z}{R_3 C_3} + \frac{V_1}{R_3 C_3}, \\ \dot{z} = -\frac{z}{R_5 C_5} - \frac{y}{R_8 C_5} - \frac{x}{R_9 C_5} + \frac{|y|^b}{R_6 C_5} + \frac{V_2}{R_7 C_5}. \end{cases} \tag{9}$$

Let the characteristic time scale be given by $\tau = R_1 C_1 = R_5 C_5 = R_9 C_5$, where one recovers the control parameters $a = \tau/(R_3 C_3)$ and $c = \tau/(R_8 C_5)$. The amplitude boosting parameter corresponds to $n = \tau/(R_6 C_5)$, while the offset boosting parameters map to $d_1 = V_1/(1\text{ V})\tau/(R_3 C_3)$ and $d_2 = V_2/(1\text{ V})\tau/(R_7 C_5)$. Nominally, $n = 1$ and $d_1 = d_2 = 0$. All parameters can, therefore, be expressed in terms of ratios of RC time constants. The corresponding circuit is shown in Figure 14, wherein the labeled voltages correspond to the state variables x, y, and z in Equation (1). Due to the inherent characteristics of the jerk system, positive integration was employed for integrating the x and y variables, while an inverse integration circuit was instantiated to integrate z. For this circuit, we initially set $R_1 = R_2 = R_3 = R_4 = R_5 = R_6 = R_7 = R_9 = 100$ kΩ, $R_8 = 167$ kΩ, and $C_1 = C_2 = C_3 = C_4 = C_5 = 1$ μF, giving $\tau = 0.1$ s and an oscillation frequency in the order of 1 Hz, $a = 1$, and $c = 0.6$ consistent with the previous sections.

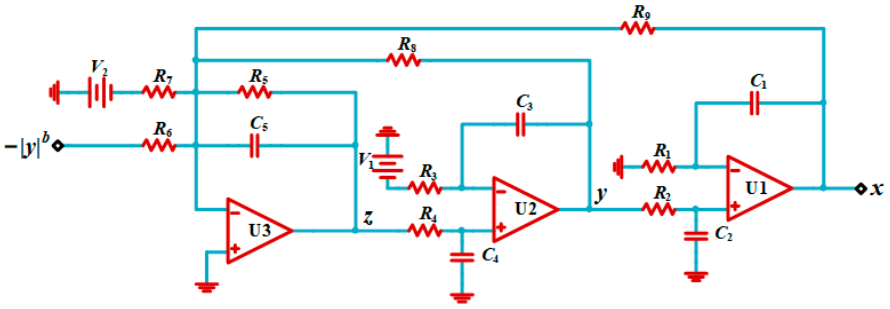

Figure 14. Simplified overall circuit realizing Equation (1).

With respect to the fractional exponentiation operation, as described in Ref. [25], the stages visible in Figure 15 implement, in order, the calculation of the absolute value, the logarithm, and the exponential functions. As long as $R_{16}/R_{19}V_p = R_{23}/R_{20}V_p = 1$ V, the exponent is given by $b = (R_{17} + R_{18})R_{22}/[R_{17}(R_{22} + R_{21})]$. Here, we set $R_{19} = R_{20} = 1.5$ MΩ, $R_{16} = R_{23} = 100$ kΩ, $V_p = 15$ V, thus fulfilling the condition. Moreover, $R_{17} = 50$ Ω, $R_{18} = 100$ Ω, $R_{21} = 20$ Ω, $R_{22} = 80$ Ω, yielding $b = 2.4$. The relatively large values of R_{19}, R_{16}, R_{20}, and R_{23} and small values of R_{17}, R_{18}, R_{21}, and R_{22} served to minimize the errors in the logarithm and exponential relationships while avoiding excessive currents and minimizing the impact of bias currents and other instabilities. The other resistors were set to $R_{10} = R_{11} = R_{12} = R_{13} = R_{14} = R_{24} = R_{25} = 10$ kΩ and $R_{15} = 1$ kΩ, alongside $V_4 = 0.6$ V, to ensure the minimum value remains above zero.

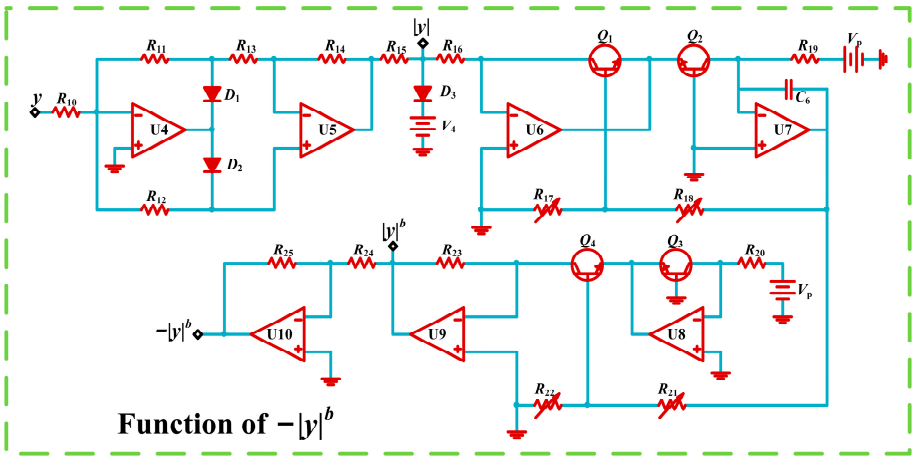

Figure 15. Circuit diagram realizing the $-|y|^b$ calculation, based on the 444 circuit detailed in Ref. [29].

All operational amplifiers were type ADA4000 or equivalent, all bipolar transistors were type 2N2222 or equivalent, and all diodes were type 1N4148 or equivalent. A dual power supply set to ±15 V was provided. Following initial experiments, it was discovered that some stages suffered from instability, leading to self-oscillation; to alleviate this problem, 1 nF capacitors were installed between the output and inverting input of U_4, U_5, U_6, U_7, U_8, and U_9. A two-layer PCB board, having a size of 80 × 80 mm, was designed, as visible in Figure 16. The voltages corresponding to the state variables were sampled at 5 kSa/s, 12-bit for 1 million points, using a digitizing oscilloscope.

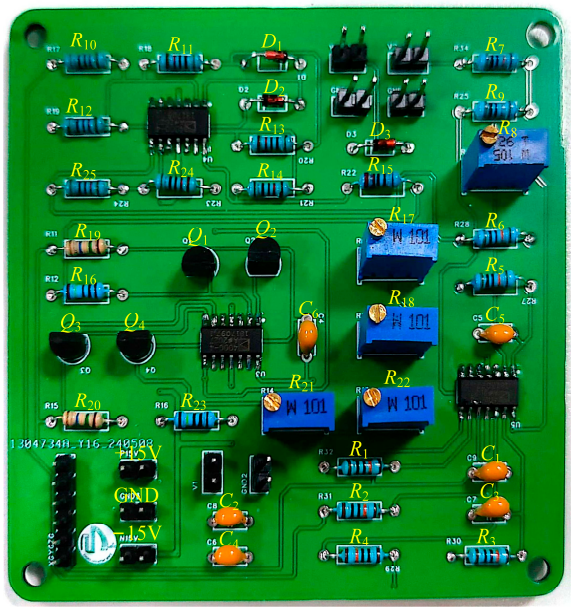

Figure 16. Photograph of the experimental realization of the system in Equation (9) in the form of an analog electronic circuit.

5.2. Results

Before investigating the dynamic behavior of the system as a function of the control and boosting parameters, the performance of the analog circuit, obtained by calculating the absolute value and fractional exponent, as shown in Figure 15, was measured. For this purpose, a triangular wave having a frequency of 7 Hz and peak-to-peak amplitude of 4 V was generated externally and supplied to R_{10}, while the output of U_9 was recorded. As visible in Figure 17, a stable and highly symmetrical response was observed. The corresponding power relationship was fitted using the Levenberg–Marquart method, yielding an estimate of 2.409 (2.405–2.414), in striking agreement with the theoretical prediction.

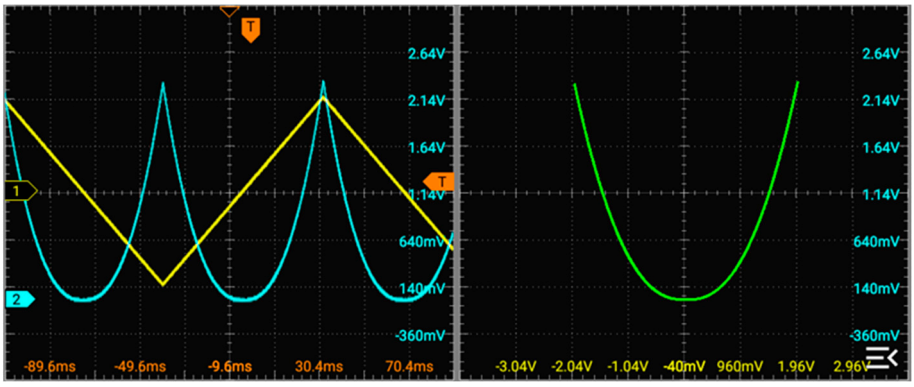

Figure 17. Experimental measurements of the input–output relationship of the analog computer subcircuit in Figure 15. (**Left** panel): time series (yellow for input and light blue for output). (**Right** panel): corresponding XY plot.

The initial investigation focused on the effect of the amplitude boosting parameter n, with the resistor R_6 being varied while maintaining the absence of any offset boosting. To preserve chaoticity, it was necessary to adjust one feedback resistor, designated as $R_8 = 141$ kΩ, resulting in $c = 0.7$. As demonstrated in Figure 18, four levels of amplitude boosting were considered, ranging from $R_6 = 45$ kΩ ($n = 2.2$) to $R_6 = 142$ kΩ ($n = 0.7$). Overall, the scaling effect was clearly evident. The morphology of the phase portraits exhibited a satisfactory degree of consistency, and there was a comparable level of agree-

ment with the results from the integration of Equation (1), as shown in Figure 1. The time series demonstrated the alternation of large and small amplitude cycles with pronounced residual periodicity, including the occurrence of sporadic bursts. It is noteworthy that at the smallest setting of n (corresponding to the largest size of the attractor), distortion became more evident, manifesting as compression of the large fluctuations in the time series and enlargement of the cavity within the chaotic orbit. For values of n below the considered range, divergence and saturation occurred, whereas, for values above it, large swings caused the onset of slow sustained self-oscillations unrelated to the chaotic dynamics.

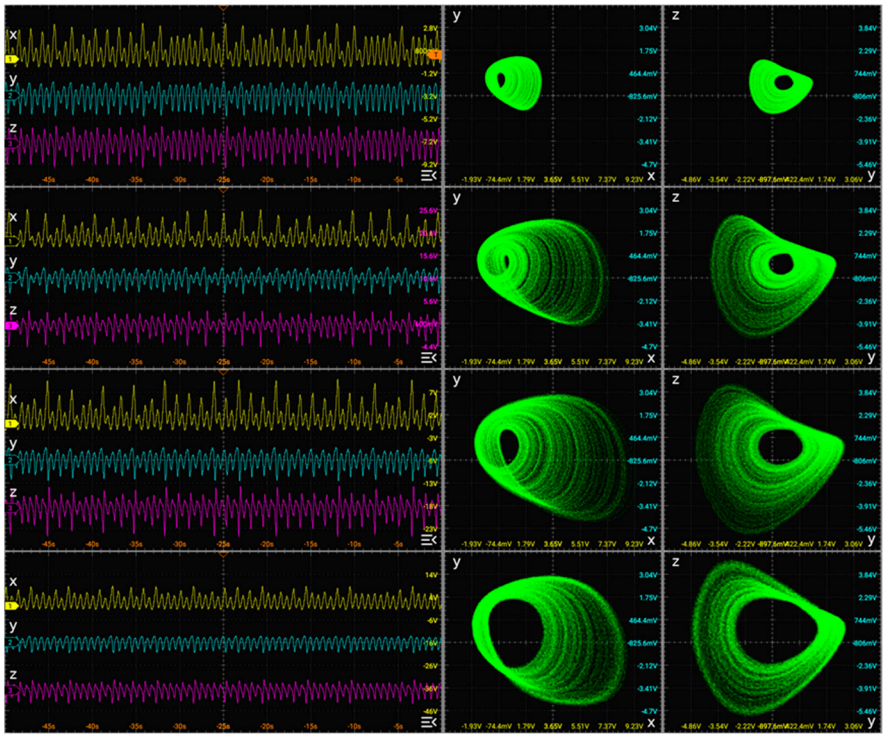

Figure 18. Experimental recordings during the application of four different levels of amplitude boosting, namely, R_6 = 45 kΩ (n = 2.2), R_6 = 94 kΩ (n = 1.1), R_6 = 118 kΩ (n = 0.8), and R_6 = 142 kΩ (n = 0.7). (**Left** panel): time series. (**Middle** and **right** panels): corresponding (x,y) and (y,z) plots.

Second, the effect of the offset boosting parameter d_2, which directly controls the variable x, was investigated by adjusting the voltage V_2 while retaining V_1 = 0 V. To retain chaoticity, it was necessary to further slightly adjust R_8 = 150 kΩ and to find a compromise between range and attractor size, giving R_6 = 69 kΩ (n = 1.45). As demonstrated in Figure 19, the analysis encompassed four levels of amplitude boosting on the x variable, ranging from V_2 = 0 V (d_2 = 0) to V_2 = −3 V (d_2 = −3). Despite minor discrepancies, the time series and phase portraits exhibited consistency with those observed in Figure 18. As the offset was increased, a marked leftward shift along the x dimension was observed. The dynamics, as evident in the time series and morphology of the phase portraits, remained largely consistent, despite the apparent shrinkage of the cavity seen in large settings. However, a notable non-ideal effect of the boosting was the generation of substantial and isolated fluctuations, classified as (super)extreme events, which resulted in the transient ejection of the trajectory from the vicinity of the attractor. For even stronger boosting, divergence eventually ensued, whereas for boosting in the opposite direction (rightward), a tendency to reduce the level of chaoticity could be noticed.

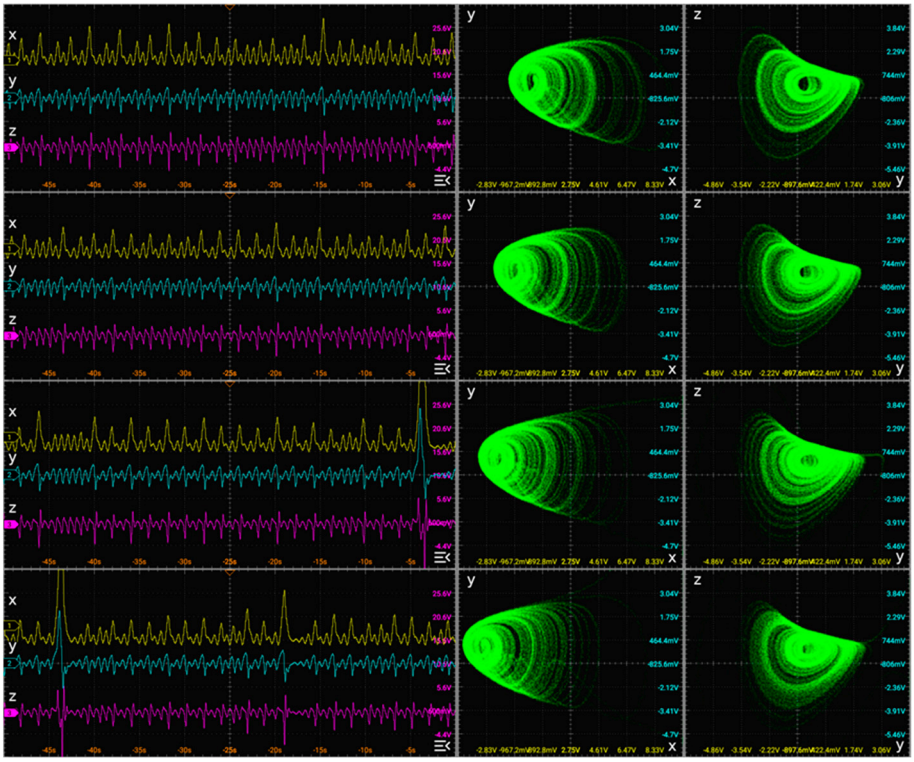

Figure 19. Experimental recordings during the application of four different levels of direct offset boosting on the x variable, namely, $V_2 = 0$ V ($d_2 = 0$), $V_2 = -1$ V ($d_2 = -1$), $V_2 = -2$ V ($d_2 = -2$), and $V_2 = -3$ V ($d_2 = -3$). (**Left** panel): time series. (**Middle** and **right** panels): corresponding (x,y) and (y,z) plots.

These findings, when considered as a whole, substantiated the viability of analog electronic fractional exponentiation within the specified framework and the effective integration of amplitude and offset boosting strategies. The deviations from ideal behaviors, which are prevalent in analog chaotic circuits, could be reasonably ascribed to the combined impact of parametric tolerances, limited precision of the amplification stages, and constraints imposed by the finite swing accessible to the system variables due to the limited power supply voltages.

6. Discussion and Conclusions

In this paper, a three-dimensional jerk system with fractional exponentiation was introduced, thus providing a novel candidate to the gallery of chaotic systems featuring the properties of amplitude control and two-dimensional interlocked offset boosting. The design of the corresponding circuit was made possible by a recently published analog computer element known as the 444 circuit, which provides fractional exponentiation by combining exponential and logarithmic operations in a compact design. A comprehensive experimental evaluation was undertaken using a physically realizable analog electronic circuit and confirmed the viability of the approach. This work exemplifies a method by which fractional exponentiation can provide an effective channel for easily re-scalable chaos generation without influencing the geometric properties of the chaotic trajectories. The proposed design may facilitate future applications of chaotic signal generators where signal versatility is important, such as in large-scale model network construction and practical scenarios such as mixing and steering control. In many cases of information processing, chaos is often used instead of true random numbers [30]. This nonlinear feedback of fractional exponentiation can be widely applied for the generation of chaos or hyperchaos in jerk systems and other dynamic systems. Therefore, we can imagine that this specific

module of the 444 circuit has significant value in chaos generation and also has great potential for the controllability design of chaos.

7. Patents

A Chinese national patent number "ZL 2024 1 0519263.7" entitled "A product operation circuit with adjustable fractional powers", covering the 444 circuit, was filed by the Nanjing University of Information Science & Technology.

Author Contributions: M.S.: Investigation, Circuit simulation, Data curation, and Writing—original draft. C.L.: Conceptualization, Methodology, Writing—review and editing, Project administration, and Funding acquisition. X.C.: Validation and Circuit implementation. M.Z.: Investigation and Writing—review and editing. Y.X.: Software and Visualization. L.M.: Writing—review and editing, Circuit implementation, Experiments, and Data collection. All authors have read and agreed to the published version of the manuscript.

Funding: This work was supported by the National Natural Science Foundation of China (Grant No.: 62371242). L.M. gratefully acknowledges the support of the Hundred Talents program of the University of Electronic Science and Technology of China, the Outstanding Young Talents Program (Overseas) of the National Natural Science Foundation of China, and the talent programs of the Sichuan province and Chengdu municipality.

Data Availability Statement: The raw time series recorded from the analog circuit using a digitizing oscilloscope are downloadable from http://dx.doi.org/10.5281/zenodo.14560396.

Conflicts of Interest: The authors declare no known competing financial interests or personal relationships that could have appeared to influence the work reported in this paper.

References

1. Yang, S.K.; Chen, C.L.; Yau, H.T. Control of chaos in Lorenz system. *Chaos Solitons Fractals* **2002**, *13*, 767–780. [CrossRef]
2. Jiang, Y.; Li, C.; Liu, Z.; Lei, T.; Chen, G. Simplified memristive Lorenz oscillator. *IEEE Trans. Circuits Syst. II Express Briefs.* **2022**, *69*, 3344–3348. [CrossRef]
3. Leonov, G.A.; Kuznetsov, N.V.; Vagaitsev, V.I. Hidden attractor in smooth Chua systems. *Phys. D Nonlinear Phenom.* **2012**, *241*, 1482–1486. [CrossRef]
4. Lin, X.; Zhou, S.; Li, H. Chaos and synchronization in complex fractional-order Chua's system. *Int. J. Bifurc. Chaos* **2016**, *26*, 1650046. [CrossRef]
5. Martínez, H.; Solís-Daun, J. Global stabilization of a bounded controlled system based on the Rössler system. *J. Frankl. Inst.* **2024**, *361*, 106692. [CrossRef]
6. Zhang, H.; Ma, X.K.; Li, M.; Zou, J.L. Controlling and tracking hyperchaotic Rössler system via active backstepping design. *Chaos Solitons Fractals* **2005**, *26*, 353–361. [CrossRef]
7. Sprott, J.C. Some simple chaotic jerk functions. *Am. J. Phys.* **1997**, *65*, 537–543. [CrossRef]
8. Tamba, V.K.; Kingni, S.T.; Kuiate, G.F.; Fotsin, H.B.; Talla, P.K. Coexistence of attractors in autonomous Van der Pol–Duffing jerk oscillator: Analysis, chaos control and synchronisation in its fractional-order form. *Pramana* **2018**, *91*, 1–11. [CrossRef]
9. Yu, S.; Lu, J.; Leung, H.; Chen, G. Design and implementation of n-scroll chaotic attractors from a general jerk circuit. *IEEE Trans. Circuits Syst. I Regul. Pap.* **2005**, *52*, 1459–1476.
10. Qin, C.; Sun, K.; He, S. Characteristic analysis of fractional-order memristor-based hypogenetic jerk system and its DSP implementation. *Electronics* **2021**, *10*, 841. [CrossRef]
11. Zhang, X.; Li, C.; Dong, E.; Zhao, Y.; Liu, Z. A conservative memristive system with amplitude control and offset boosting. *Int. J. Bifurc. Chaos* **2022**, *32*, 2250057. [CrossRef]
12. Li, C.; Sprott, J.C. Amplitude control approach for chaotic signals. *Nonlinear Dyn.* **2013**, *73*, 1335–1341. [CrossRef]
13. Wu, Q.; Hong, Q.; Liu, X.; Wang, X.; Zeng, Z. A novel amplitude control method for constructing nested hidden multi-butterfly and multiscroll chaotic attractors. *Chaos Solitons Fractals* **2020**, *134*, 109727. [CrossRef]
14. Du, C.; Liu, L.; Zhang, Z.; Yu, S. A mem-element wien-bridge circuit with amplitude modulation and three kinds of offset boosting. *Chaos Solitons Fractals* **2022**, *165*, 112832. [CrossRef]
15. Zhang, X.; Li, C.; Huang, K.; Liu, Z.; Yang, Y. A chaotic oscillator with three independent offset boosters and its simplified circuit implementation. *IEEE Trans. Circuits Syst. II Express Briefs* **2023**, *71*, 51–55. [CrossRef]

16. Minati, L. Across neurons and silicon: Some experiments regarding the pervasiveness of nonlinear phenomena. *Acta Phys. Pol. B.* **2018**, *49*, 2029–2094. [CrossRef]
17. Chua, L.O. Chua circuit. *Scholarpedia* **2007**, *2*, 1488. [CrossRef]
18. Wang, G.Y.; Zheng, Y.; Liu, J.B. A hyperchaotic Lorenz attractor and its circuit implementation. *Acta Phys. Sin.* **2007**, *56*, 3313–3319.
19. Chen, Y.; Lai, Q.; Zhang, Y.; Erkan, U.; Toktas, A. Complex dynamics of a new multiscroll memristive neural network. *Nonlinear Dyn.* **2024**, *112*, 8603–8616. [CrossRef]
20. Bao, B.; Chen, L.; Bao, H.; Xu, Q.; Chen, M.; Wu, H. Burst patterns with Hopf bifurcation in a simplified FHN circuit. *Nonlinear Dyn.* **2024**, *112*, 10373–10390. [CrossRef]
21. Lai, Q.; Wan, Z.; Kengne, L.K.; Kuate, P.D.K.; Chen, C. Two-memristor-based chaotic system with infinite coexisting attractors. *IEEE Trans. Circuits Syst. II Express Briefs* **2020**, *68*, 2197–2201. [CrossRef]
22. Li, C.; Wang, D. An attractor with invariable Lyapunov exponent spectrum and its Jerk circuit implementation. *Acta Phys. Sin.* **2009**, *58*, 764.
23. Wu, J.; Li, C.; Ma, X.; Lei, T.; Chen, G. Simplification of chaotic circuits with quadratic nonlinearity. *IEEE Trans. Circuits Syst. II Express Briefs* **2021**, *69*, 1837–1841. [CrossRef]
24. Rajagopal, K.; Akgul, A.; Jafari, S.; Karthikeyan, A.; Çavuşoğlu, Ü.; Kacar, S. An exponential jerk system: Circuit realization, fractional order and time delayed form with dynamical analysis and its engineering application. *J. Circuits Syst. Comput.* **2019**, *28*, 1950087. [CrossRef]
25. Adelakun, A.O.; Ogunjo, S.T. Active control and electronic simulation of a novel fractional order chaotic jerk system. *Commun. Nonlinear Sci. Numer. Simul.* **2024**, *130*, 107734. [CrossRef]
26. Xu, Q.; Ding, X.; Wang, N.; Chen, B.; Parastesh, F.; Chen, M. Spiking activity in a memcapacitive and memristive emulator-based bionic circuit. *Chaos Solitons Fractals* **2024**, *187*, 115339. [CrossRef]
27. Sprott, J.C. *Elegant Chaos: Algebraically Simple Chaotic Flows*; World Scientific: Singapore, 2010.
28. Minati, L.; Gambuzza, L.V.; Thio, W.J.; Sprott, J.C.; Frasca, M. A chaotic circuit based on a physical memristor. *Chaos Solitons Fractals* **2020**, *138*, 109990. [CrossRef]
29. Cen, X.; Li, C.; Liu, W.; Yang, Y.; Minati, L. A Novel Analog Electronic Circuit for Versatile Fractional Exponentiation. *Int. J. Bifurc. Chaos* 2025, *in press*.
30. Amirany, A.; Mohebbi, L. SQTRNG: Spintronic Quaternary True Random Number Generator. In *Spin*; World Scientific Publishing Company: Singapore, 2024.